


Theoretical study of GaN (0001) surface reconstructions and La and Ga adatoms under N- and Ga-rich conditions

Fatima Al-Quaiti¹ and Alexander A. Demkov^{2,*}

¹*Department of Chemistry, The University of Texas, Austin, Texas 78712, USA*

²*Department of Physics, The University of Texas, Austin, Texas 78712, USA*

 (Received 29 June 2020; revised 27 February 2021; accepted 16 March 2021; published 5 April 2021)

Using density functional theory, we determined that 2×2 and $(\sqrt{3}\times\sqrt{3})R30^\circ$ surface reconstructions of bulk-terminated GaN (0001) are degenerate in energy but differ in their electronic structure. Consistent with previous reports, our study of the adsorption energy of Ga adatoms shows that a laterally contracted Ga bilayer is the most energetically favorable surface arrangement under Ga-rich conditions, albeit with a different atomic arrangement of the Ga bilayer than previously reported. We also determined the potential energy surfaces for La and Ga adatoms on bulk-terminated GaN (0001) surface and for a La adatom on a bulk-terminated GaN (0001) covered by a contracted Ga bilayer and discuss possible adatom surface migration paths. An exchange reaction of a La adatom with surface Ga was found to be energetically favorable for both the bulk-terminated and the Ga bilayer-covered surfaces, indicating formation of LaN. A careful study of the diffusion of a La adatom through the Ga bilayer toward the bulk-terminated GaN surface suggests that a lower energy arrangement is achieved when the La adatom exchanges positions with a surface Ga atom. This indicates that LaGa₂ and LaN are potential materials to form a transition layer to facilitate epitaxial integration of oxides on GaN.

DOI: [10.1103/PhysRevMaterials.5.044602](https://doi.org/10.1103/PhysRevMaterials.5.044602)

I. INTRODUCTION

Gallium nitride (GaN) is a semiconductor used in high-frequency, high-power, and high-temperature electronics due to its large band gap, high electron mobility, and high operating temperature [1–3]. However, GaN-based high-electron mobility transistors (HEMTs) are limited by their relatively high gate leakage [4]. One possible solution to this issue is the addition of metal-oxide-semiconductor (MOS) or metal-insulator-semiconductor (MIS) structures to form MOS-HEMTs or MIS-HEMTs that would have lower gate leakage and higher breakdown fields [4]. These would enable GaN-based transistors to have more efficient power consumption and better power generation to make more practical and economical devices.

Rare-earth oxides (REOs) serve as good candidates for the gate dielectric in MOS-HEMTs due to their chemical [5] and thermal [6] stability and good optical and electrical properties [7,8]. Successful growth of REOs, such as Er₂O₃ [9], Eu₂O₃ [10], La₂O₃ [11], Gd₂O₃ [12], and Sc₂O₃ [13], on GaN has been reported. However, in some cases, there are fixed charge effects at the interface which present challenges for applications [14,15]. Additionally, wetting of REOs on GaN can be problematic because bonding in GaN is largely covalent and, contrastingly, bonding in REOs is mostly ionic. This stark difference in chemical behavior destabilizes the interface. To achieve wetting, the interface energy must be lowered. Hence, it is necessary to determine a transition layer

that can accommodate covalent and ionic bonds and lower the interfacial energy.

This transition layer can be made using a metal nitride layer, such as TiN or ScN, which have been previously integrated with GaN [16], or NbN, which can facilitate high-temperature annealing by inhibiting GaN decomposition [17]. The transition can also be achieved using Zintl intermetallics, which are a class of metal compounds with the chemical formula AB_2 , where A is an electropositive group 1 or 2 metal and B is an electronegative group 13–16 metal [18]. Lanthanum digallide (LaGa₂) is one potential material to form a Zintl-Klemm transition layer. To test the feasibility of integrating LaGa₂ on GaN, it is first necessary to understand the chemical behavior of La on the GaN surface.

The GaN surface structure is sensitive to the presence of excess Ga or N during growth. Under N-rich conditions, the GaN surface has been reported to be Ga terminated. However, growth under N-rich conditions yields a rough surface and poor-quality film. When grown under Ga-rich conditions, the surface is smoother and higher quality [19]. Experimental studies suggest that growth under Ga-rich conditions results in 2–3 ML of excess Ga on the surface [20]. This surface shows a fluidlike behavior, suggesting a resemblance to bulk Ga metal, with Ga following the GaN surface corrugation, as measured by scanning tunneling microscopy (STM), but shows distinct higher-order reflections in reflection high-energy electron diffraction and has been hence dubbed “ 1×1 ” (pseudo 1×1). STM on the GaN surface can only provide a time-averaged configuration of the Ga atoms at the surface [20,21] because the time scale of STM is too slow to measure the rapid movement of the surface Ga. There have been several theoretical studies of the surface morphology of Ga-rich GaN

*demkov@physics.utexas.edu

(0001) [21–24]. The $(\sqrt{3}\times\sqrt{3})R30^\circ$ GaN (0001) structure with a laterally contracted Ga bilayer is currently the most widely accepted model for the GaN (0001) surface grown in a Ga-rich environment.

In this paper, we use supercell surface slab calculations in the framework of density functional theory (DFT) to compare relaxed $(\sqrt{3}\times\sqrt{3})R30^\circ$ with 2×2 GaN (0001) surfaces under N-rich conditions to determine if they support unique surface reconstructions. To determine the likelihood of forming LaGa_2 or LaN transition layers, we consider the interaction of a La adatom with the GaN surface. We also investigate the adsorption energy of Ga adatoms at the surface. The adsorption of La on the laterally contracted Ga bilayer-covered GaN (0001) surface, corresponding to Ga-rich conditions, is also studied, and we determine whether the atomic arrangement of the laterally contracted Ga bilayer is sensitive to the choice of exchange correlation functional.

II. METHODS

DFT, as implemented in the Vienna *ab initio* Simulation Package (VASP) code, was used to perform all calculations [25]. The Perdew-Burke-Ernzerhof (PBE) generalized-gradient approximation (GGA) and local density approximation (LDA) were used for the exchange correlation energy functional. We used projector-augmented-wave potentials to describe La, Ga, and N and a cutoff energy of 600 eV [26]. The valence electron configurations considered were $5s^2 5p^6 6s^2 5d^1$ for La, $4s^2 3d^{10} 4p^1$ for Ga, and $2s^2 2p^3$ for N. Each self-consistent electronic calculation was converged to within 10^{-6} eV per cell, and the ionic relaxation was iterated until the forces were < 0.01 eV/Å. For the Brillouin zone integration of bulk La (space group $P6_3/mmc$), a $10\times 10\times 6$ Γ -centered grid was used. For bulk Ga (space group $Abma$), a $12\times 12\times 12$ Monkhorst-Pack k-point mesh was used. For ionic relaxation of the bulk structure of GaN (space group $P6_3mc$), we used a Γ -centered $8\times 8\times 8$ k-point grid, and for the $(\sqrt{3}\times\sqrt{3})R30^\circ$, $(\sqrt{3}\times 2\sqrt{3})R30^\circ$, and $(2\sqrt{3}\times 2\sqrt{3})R30^\circ$ GaN (0001) slabs, we used $8\times 8\times 1$, $8\times 4\times 1$, and $4\times 4\times 1$ Γ -centered grids, respectively. We used a $10\times 10\times 1$ grid for density of states (DOS) calculations of the $(\sqrt{3}\times\sqrt{3})R30^\circ$ GaN (0001) slab.

The lattice parameters calculated using GGA for bulk wurtzite GaN were $a = b = 3.22$ Å, $c = 5.24$ Å, and $u = 0.377$, and those calculated using LDA were $a = b = 3.15$ Å, $c = 5.14$ Å, and $u = 0.376$, which compare favorably with the experimental values of $a = b = 3.19$ Å, $c = 5.19$ Å, and $u = 0.377$ [27,28] and theoretical values of $a = b = 3.22$ Å, $c = 5.23$ Å, and $u = 0.380$ for GGA [29] and $a = b = 3.143$ Å, $c = 5.11$ Å, and $u = 0.377$ for LDA [30]. The band gap of GaN calculated using the GGA and LDA functionals were found to be 1.8 and 2.5 eV, respectively. Both are comparable with previous calculations which are 1.8 eV for GGA [29] and 2.26 eV for LDA [24]. Both underestimate the experimental band gap of 3.4 eV [19], as is typical of both LDA and GGA. To investigate the surface properties and the effects of adatoms on the GaN surface, we employed a $(\sqrt{3}\times\sqrt{3})R30^\circ$ GaN (0001) slab consisting of 8 GaN bilayers and 15 Å of vacuum, as shown in Figs. 1(a) and 1(b). The GaN (0001) top surface is Ga-terminated, and the bottom surface is terminated with

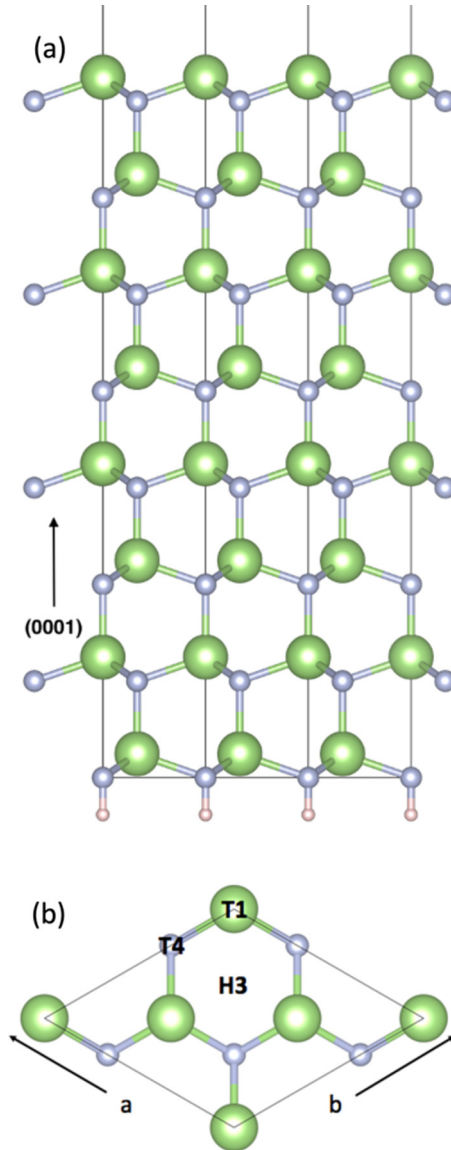


FIG. 1. The bottom surface is passivated with pseudo-H, shown as pink spheres. The (a) side view and (b) top view of the ideally terminated $(\sqrt{3}\times\sqrt{3})R30^\circ$ GaN (0001) slab. The large green spheres and small gray spheres are Ga and N atoms, respectively. T1, T4, and H3 are the Ga top site, N top site, and hollow site, respectively.

N. At the bottom surface, the N dangling bonds are passivated with pseudohydrogen atoms with charge of $0.75 e^-$ to restore the bulklike behavior in the slab. Due to the polar nature of GaN, the resulting electric field would violate the periodic boundary condition in the direction normal to the surface; to avoid this problem, we implemented a dipole correction in our calculations. Crystal structures and figures are visualized using the VESTA visualization program.

III. RESULTS AND DISCUSSION

A. Atomic relaxation

Two cells commonly used to model the GaN (0001) surface are the $(\sqrt{3}\times\sqrt{3})R30^\circ$ and 2×2 cells [21–23,29,31,32]. A 2×2 reconstruction is observed when GaN is grown using

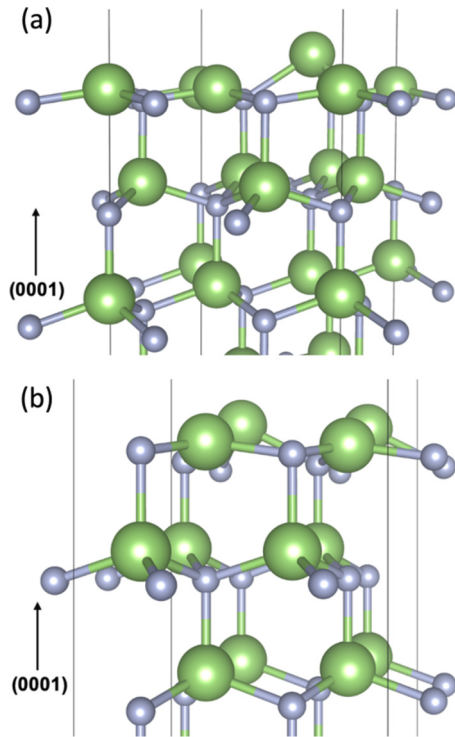


FIG. 2. Surface reconstructions for (a) $(\sqrt{3} \times \sqrt{3})R30^\circ$ GaN (0001) (b) 2×2 GaN (0001). The large green spheres and small gray spheres are Ga and N atoms, respectively.

molecular beam epitaxy (MBE) and has been theoretically demonstrated to be a distinct surface reconstruction [19]. A $(\sqrt{3} \times \sqrt{3})R30^\circ$ cell is typically employed for models that include a Ga bilayer on the surface, which is energetically like the 1×6 Ga bilayer, which supports the low-energy electron diffraction (LEED) pattern observed in experiment [33]. We compared the surface reconstructions of the $(\sqrt{3} \times \sqrt{3})R30^\circ$ with 2×2 structures to determine the possible differences in surface morphology.

We begin our analysis by comparing the surface reconstruction of bulk-terminated $(\sqrt{3} \times \sqrt{3})R30^\circ$ GaN (0001) using GGA and LDA to determine the sensitivity of the surface relaxation to the exchange correlation functional. The $(\sqrt{3} \times \sqrt{3})R30^\circ$ GaN (0001) cell has three Ga atoms in the surface layer, as shown in Fig. 2(a). In this cell, 1 ML consists of three Ga atoms. For the surface reconstruction found using the GGA functional, 1 of the 3 Ga atoms in the surface layer is displaced upward by 0.61 \AA , and the other two Ga atoms are displaced downward by 0.29 \AA . Similarly, in the surface reconstruction found using the LDA functional, one of the surface Ga atoms is displaced upward by 0.5 \AA , and the other two Ga atoms are displaced downward by 0.2 \AA . For both LDA and GGA, we found that any 1 of the 3 surface Ga atoms may be displaced upward, as the three surface Ga atoms are equivalent. The atomic and electronic properties of the GaN (0001) surface are independent of which Ga atom is displaced upward, and overall, the surface reconstruction is independent of whether the LDA or GGA functional is used. This gives us confidence that the surface properties under investigation are not a strong function of the choice of exchange correlation

functional. The surface layer of the 2×2 GaN (0001) cell contains four Ga atoms, as shown in Fig. 2(b). In this cell, 1 ML consists of four Ga atoms. Using GGA for ionic relaxation, the surface reconstruction is characterized by two atoms displaced upward by 0.42 \AA and two atoms displaced downward by 0.24 \AA , which is comparable with previously reported results for the 2×2 GaN surface reconstruction [29]. The displacement of surface Ga atoms is similar in the 2×2 and $(\sqrt{3} \times \sqrt{3})R30^\circ$ reconstructions. To properly compare the total energy of the two reconstructions, we must employ a larger supercell.

Due to the difference in the number of Ga atoms in 1 ML in $(\sqrt{3} \times \sqrt{3})R30^\circ$ and 2×2 GaN (0001), we cannot directly compare the energy of the two surface reconstructions. To do this without needing to use the chemical potential, we use the $(2\sqrt{3} \times 2\sqrt{3})R30^\circ$ [Fig. 3(a)] and GaN (0001) $(\sqrt{3} \times 2\sqrt{3})R30^\circ$ GaN (0001) [Fig. 3(b)] slabs, both of which would allow one to observe both the $(\sqrt{3} \times \sqrt{3})R30^\circ$ and 2×2 GaN (0001) surface reconstructions. The $(\sqrt{3} \times 2\sqrt{3})R30^\circ$ GaN (0001) and $(2\sqrt{3} \times 2\sqrt{3})R30^\circ$ GaN (0001) slabs have 6 and 12 Ga atoms comprising the surface Ga layer, respectively. We performed two ionic relaxations for each structure with the initial structures oriented as either the $(\sqrt{3} \times \sqrt{3})R30^\circ$ or 2×2 GaN (0001) surface reconstructions, for a total of four calculations.

For both the $(\sqrt{3} \times 2\sqrt{3})R30^\circ$ and $(2\sqrt{3} \times 2\sqrt{3})R30^\circ$ cells, the final arrangements resembled the initial arrangements and remained in either the 2×2 or $(\sqrt{3} \times \sqrt{3})R30^\circ$ reconstructions. We found that the $(\sqrt{3} \times \sqrt{3})R30^\circ$ arrangement was very slightly lower in energy than the 2×2 arrangement by $5.02 \times 10^{-3} \text{ eV/\AA}^2$. Hence, we conclude that, based on our calculations, the surface reconstruction of bulk-terminated GaN (0001) can resemble that of either the 2×2 or $(\sqrt{3} \times \sqrt{3})R30^\circ$ arrangements, where the exact experimental realization likely depends on surface preparation conditions.

B. Electronic structure

We now consider the electronic structure of the $(\sqrt{3} \times \sqrt{3})R30^\circ$ reconstruction and compare it with that of the 2×2 reconstruction, previously calculated with similar methods by Shin *et al.* [29]. The DOS for the top three layers of unrelaxed and relaxed $(\sqrt{3} \times \sqrt{3})R30^\circ$ structure are shown in Figs. 4(a) and 4(b), respectively. The partial DOS below the third GaN layer resembles that of bulk GaN; hence, we have omitted the lower layers in Figs. 4(a) and 4(b). The DOS for the $(\sqrt{3} \times \sqrt{3})R30^\circ$ and the 2×2 reconstructions both show surface states that are in the top GaN bilayers. These states are mostly *s*- and *p*-like in the Ga layer and *p*-like in the N layer. The Fermi level crosses the surface band, indicating the surface is metallic. After relaxation, the surface band splits to form a 1.8 eV gap below the Fermi level. The partial charge density before relaxation indicates the charge density is distributed among all surface Ga atoms. The hybridization is consistent with *s* and *p_z* hybridization, like the charge distribution of surface Ga atoms in the 2×2 reconstruction [29]. After relaxation, the charge is mostly concentrated on the Ga atom that is displaced upward. The lower Ga atoms have considerably less charge, suggesting that charge is transferred from the lower surface Ga atoms to the higher Ga atom to occupy lower energy states. Again, this is

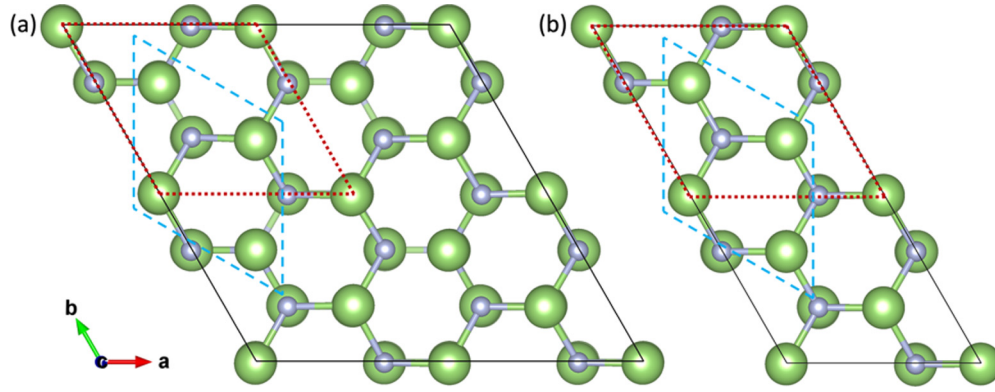


FIG. 3. Top view of (a) $(2\sqrt{3}\times 2\sqrt{3})R30^\circ$ GaN (0001) and (b) $(\sqrt{3}\times 2\sqrt{3})R30^\circ$ GaN (0001) slabs. The 2×2 unit cell is outlined with a blue dashed line, and the $(\sqrt{3}\times 2\sqrt{3})R30^\circ$ unit cell is outlined with a red dotted line. The large green spheres and small gray spheres are Ga and N atoms, respectively.

like the charge distribution of the raised Ga atoms in the 2×2 reconstruction [29]. Below the Fermi level, the surface states remain largely *s*- and *p*-like in the Ga layer and *p*-like in the N layer. Above the Fermi level, the surface states for both the Ga and N layers are *p*-like. The Fermi level still crosses the surface band, indicating the surface remains metallic after relaxation.

We use Bader charge analysis to visualize the charge distribution at the surface of the $(\sqrt{3}\times\sqrt{3})R30^\circ$ GaN slab. Using the GGA exchange correlation functional, we find that the bulk Ga atoms lose $1.54 e^-$. The lower two surface Ga atoms lose $1.46 e^-$, and the surface Ga atom that is displaced upward loses only $0.57 e^-$. Bulk N atoms gain $1.57 e^-$, and the surface N atoms gain $1.47 e^-$. Using the LDA exchange correlation functional, we observe bulk Ga atoms lose $1.47 e^-$ of charge, while the two lower surface Ga atoms lose $1.39 e^-$, and the Ga atom which is displaced upward only loses $0.60 e^-$. The surface and bulk N atoms lose $1.47 e^-$. Regardless of the exchange correlation functional used, our results suggest that

the Ga atom that is displaced upward has greater charge than that of bulk and other surface Ga atoms.

C. Single Ga and La adatom surface diffusion on $(\sqrt{3}\times\sqrt{3})R30^\circ$ GaN surface

We now consider the diffusion of Ga and La adatoms on the GaN surface under N-rich conditions, i.e., the bulk-terminated surface. First, we determine the potential energy surface (PES) for a single Ga adatom on the GaN surface, which is shown in Fig. 5(a). We construct a 6×6 grid on the $(\sqrt{3}\times\sqrt{3})R30^\circ$ GaN (0001) simulation surface and add high-symmetry T1, T4, and H3 sites as well. Then a Ga adatom is placed at each grid point and allowed to relax along the *z* axis, while the rest of the atoms are completely free. To generate the PES, we plot the relative energy of such configurations as a function of the Ga adatom position. We find that the N top sites, labeled T4 in Fig. 1(b), are the most energetically favorable sites for Ga adsorption, and the Ga top sites, labeled T1, are the least

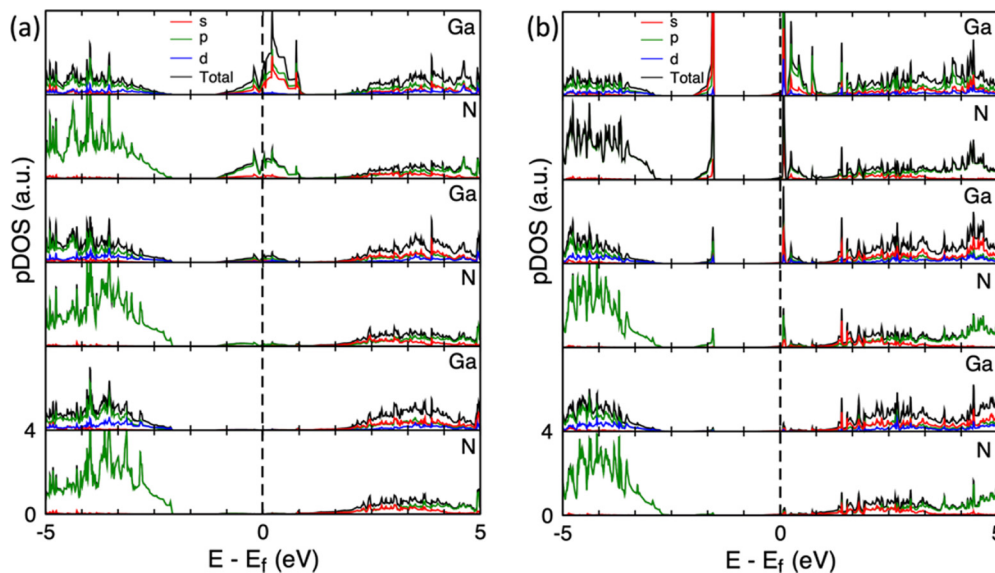


FIG. 4. Density of states for the top three GaN bilayers of the $(\sqrt{3}\times\sqrt{3})R30^\circ$ GaN (0001) slab (a) before relaxation (b) and after relaxation.

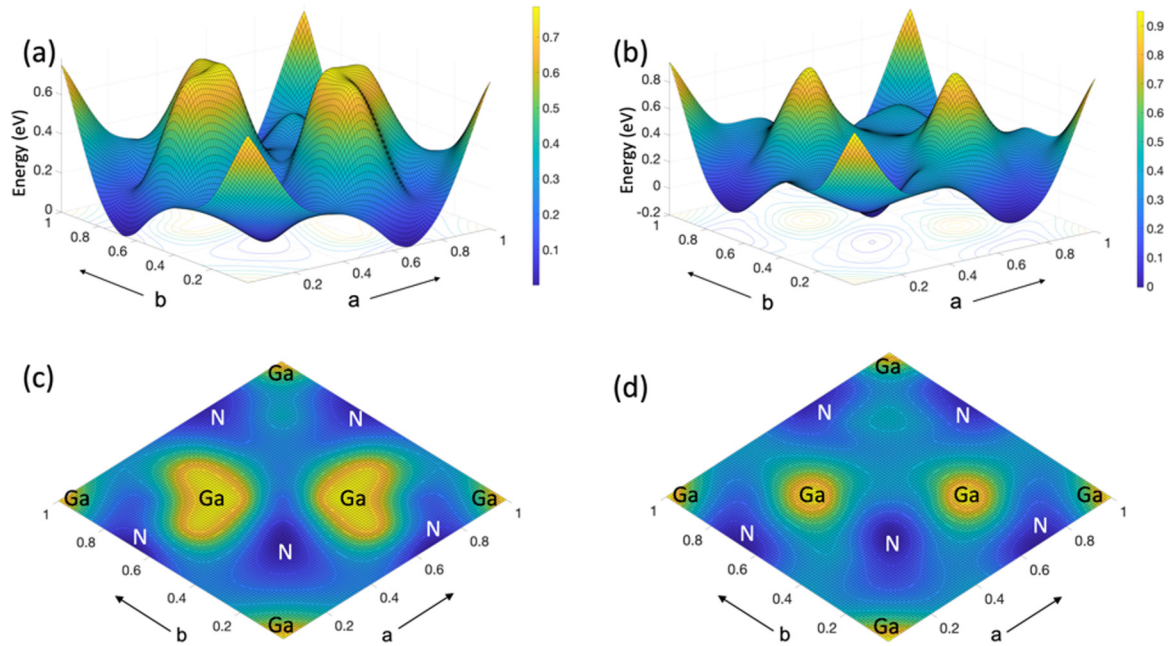


FIG. 5. Potential energy surface plot for (a) a Ga adatom and (b) a La adatom on $(\sqrt{3}\times\sqrt{3})R30^\circ$ GaN (0001) and contour plots and for (c) a Ga adatom and (d) a La adatom on $(\sqrt{3}\times\sqrt{3})R30^\circ$ GaN (0001). The lowest energy configuration is defined as 0 eV.

energetically favorable, which has similarly been reported for Eu, Ce, and Gd [29], Al [34], Y [35], B [31], Sc [36], and V [37]. The hollow site, labeled H3, is found to be lower in energy than T1. Upon the addition of the Ga adatom, the surface layer of the GaN (0001) surface becomes flat, as it would with an ideal bulk termination. The spacing between the surface Ga atoms and the Ga adatom ranges from 2.5 to 2.7 Å, which is comparable with the 2.4–2.8 Å range in bulk Ga metal [38].

Similarly, we calculate the PES of a La adatom on the GaN (0001) surface, which is shown in Fig. 5(b), using the same method described above for the Ga adatom PES. We find that the PES looks like that of Ga. The N top sites are the most energetically favorable for La adsorption, and the Ga top sites are the least energetically favorable. The N atom below the La adatom is displaced upward by 0.3 Å, and the surface Ga atom, which was originally 0.5 Å above the others, is displaced 0.36 Å downward and away from the La atom along the a and b directions, likely due to the large size of the La adatom. The average distance between the La adatom and the three adjacent Ga atoms is 2.9 Å. This is significantly shorter than the average distance of 3.35 Å between La and Ga in bulk Zintl intermetallic LaGa_2 [39]. The distance between La and the underlying N atom is 2.26 Å, which is shorter than the average La-N bond length of 2.65 Å in LaN [40].

We find that both Ga and La are attracted to the underlying N, and both are repelled by Ga. The potential energy difference between the T1 and T4 sites is 0.75 eV for Ga and 0.95 eV for La. The diffusion rate is calculated using the formula $1/\tau = \nu e^{-E/k_B T}$, where τ is the diffusion rate, ν is the attempt frequency (we assume $\nu \approx 10^{12} \text{ s}^{-1}$, which is typically used for the frequency of atomic vibration [41]), E is the potential energy barrier, k_B is Boltzmann's constant, and T is temperature. At room temperature, the diffusion rates are on the order of 1 s for Ga and 10^3 s for La. At

750 °C, the diffusion rates are 10^{-9} and 10^{-8} s for Ga and La, respectively. We compare these diffusion rates with that of the rare-earth atoms Eu, Gd, and Ce [29]. For a transition from T4 to T1, the diffusion rates are on the order of 10^{-2} , 10^{11} , and 10^{13} s at room temperature, and 10^{-10} , 10^{-7} , and 10^{-5} s at 750 °C for Eu, Ce, and Gd, respectively. Diffusion is relatively slow for all adatoms along this path. The diffusion rates for the path from H3 to T4 are listed in Table I. For the Ga adatom, we find that there is no potential energy barrier between the H3 and T4 sites, in contrast to a previous report which suggested the existence of a diffusion barrier of 0.4 eV and that the two sites are energetically degenerate [42]. The diffusion barrier reported by Zywietz *et al.* [42] was calculated using LDA; however, they report differences of ≤ 0.1 eV when comparing with equivalent calculations using GGA [43]. In our case, we instead find that diffusion would occur between T4 sites where the potential energy barrier is 0.25 eV. The diffusion rates for a Ga atom moving from one T4 site to another are 10^{-8} and 10^{-11} s at room temperature and 750 °C, respectively. The results of a climbing nudged elastic band (cNEB) [44] calculation support the results of the PES and show no barrier between the H3 and T4 sites. The barrier height for the La adatom moving from H3 to T4 is 0.06 eV, and the diffusion rates are on the order of 10^{-11} and 10^{-12} s at room temperature and 750 °C, respectively. In the reverse direction when the La adatom moves from T4 to H3, the PES result shows a transition barrier of 0.35 eV, and the cNEB result shows a barrier of approximately 0.4 eV. With a barrier height of 0.4 eV, the diffusion rates are on the order of 10^{-5} and 10^{-10} s at room temperature and 750 °C, respectively. The radius of La is comparable with that of Ga, which could explain the relatively fast diffusion rates. It is apparent that diffusion along H3 and T4 sites is more likely than diffusion along the T1 site because the diffusion rates are significantly faster. This suggests that the diffusion of Ga and rare-earth

TABLE I. Properties of metal atoms.

Adatom	Ga	La	Eu	Ce	Gd
Electronegativity (χ)	1.81	1.10	1.12	1.20	1.20
$\delta(\chi_{\text{Ga}} - \chi_{\text{Metal}})$	0	0.70	0.69	0.61	0.61
Metal-Ga distance (DFT) (\AA)	2.53 ^a	3.35 ^a	2.96 ^b	3.11 ^b	2.88 ^b
Metal-Ga distance (experiment) (\AA) ^c	2.44 ^c	3.33 ^d	3.37 ^e	3.31 ^e	3.20 ^e
Covalent radius (\AA)	1.22	2.07	1.98	2.04	1.96
Diffusion rate from H3 to T4 at 23 °C (s)	–	$10^{-11\text{a}}$	$10^{-7\text{b}}$	$10^{-2\text{b}}$	$10^{-2\text{b}}$
Diffusion rate from H3 to T4 at 750 °C (s)	–	$10^{-12\text{a}}$	$10^{-11\text{b}}$	$10^{-10\text{b}}$	$10^{-10\text{b}}$

^aThis work.^bRef. [29].^cRef. [38].^dRef. [39].^eRef. [48].

adatoms on the GaN surface is directionally dependent based on the underlying surface atoms.

D. Single Ga and La adatom surface exchange on $(\sqrt{3} \times \sqrt{3})R30^\circ$ GaN surface

In the lowest energy configuration, the La adatom is equidistant from all three surface Ga atoms [Fig. 6(a)]. We calculate the relative energy of a “flipped structure,” in which

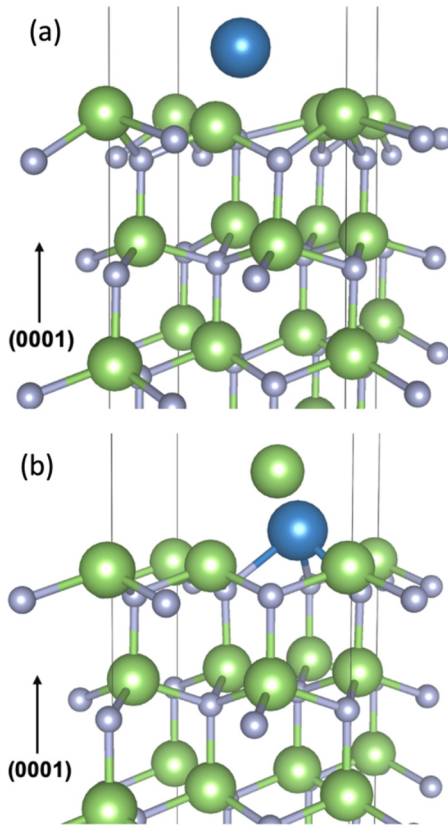


FIG. 6. The large green spheres, small gray spheres, and large blue sphere are Ga, N, and La atoms, respectively. The $(\sqrt{3} \times \sqrt{3})R30^\circ$ GaN (0001) surface (a) with a La adatom on top of the surface and (b) with the La adatom exchanging positions with a surface Ga atom.

the position of the La adatom is exchanged with each of the three surface Ga atoms [Fig. 6(b)]. Unsurprisingly, there is no significant energy difference regarding which surface Ga atom participates in the exchange. However, we find that, when La is exchanged with any of the adjacent surface Ga atoms, the energy of the system decreases by 1.73 eV, suggesting a strong preference for the flipped structure. This is like the results for Eu, Ce, and Gd [29], Al [34], Y [35], B [31], Sc [36], and V [37], in which an exchange between the metal adatom with a surface Ga atom resulted in a lower energy structure. A cNEB calculation shows a potential barrier height of 0.75 eV for the exchange. After the exchange, the distance between the La and Ga atoms is ~ 3.2 \AA , which is like the average La-Ga distance of 3.35 \AA in LaGa_2 . The distance between the La and N atoms in LaN is ~ 2.65 \AA [40], which is slightly larger than the La-N bond distance of 2.35 \AA after the exchange. Bader charge analysis shows that the La atom loses $1.66 e^-$ of charge. The two remaining surface Ga atoms lose $1.05 e^-$, and the displaced Ga atom loses $1.18 e^-$ compared with $1.52 e^-$ lost by Ga in bulk GaN. The surface N atoms show no significant difference in charge distribution. Based on the Bader analysis and partial charge distribution shown in Fig. 7(b), these results suggest that charge is transferred from the La atom to the adjacent N atoms, indicating the formation of LaN on the surface. The Ga atoms which remain in the GaN layer donate charge to the Ga atom which participated in the exchange. We also study a surface exchange reaction between a Ga adatom and a surface Ga atom. The initial and final states are both the lowest energy configuration for a Ga adatom on the $(\sqrt{3} \times \sqrt{3})R30^\circ$ surface, the T4 site. We determine a 1.70 eV energy barrier for a Ga adatom to exchange positions with a surface Ga atom.

E. Single Ga and La adatom surface diffusion on $(2\sqrt{3} \times 2\sqrt{3})R30^\circ$ GaN surface

We now repeat the study of adatom surface diffusion on the $(2\sqrt{3} \times 2\sqrt{3})R30^\circ$ GaN surface to check if the $(\sqrt{3} \times \sqrt{3})R30^\circ$ surface cell is large enough to observe adatom diffusion without interaction with the images in neighboring cells. The $(\sqrt{3} \times \sqrt{3})R30^\circ$ GaN (0001) surface flattens and resembles the ideal bulk termination after a Ga or La adatom is placed on the surface [Fig. 6(a)]. Interestingly, the

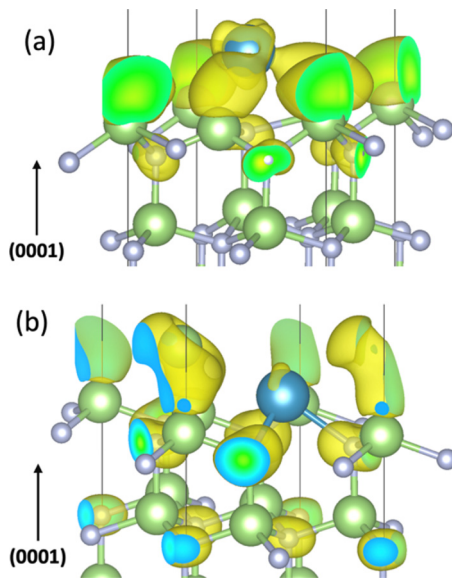


FIG. 7. The large green spheres, small gray spheres, and large blue sphere are Ga, N, and La atoms, respectively. Partial charge density of the occupied states for (a) a La adatom on the $(\sqrt{3} \times \sqrt{3})R30^\circ$ GaN (0001) slab and (b) a La adatom exchanged with a surface Ga atom. La is the large blue sphere.

$(2\sqrt{3} \times 2\sqrt{3})R30^\circ$ surface did not flatten with the addition of a Ga or La adatom, which results in two distinct Ga top sites and two distinct Ga bridge sites which differ by whether adjacent Ga atoms are displaced upward after surface relaxation. Rather than calculating the entire PES, we mapped the diffusion of the adatom along a path which includes both Ga top sites and both Ga bridge sites, as shown in Fig. 8(a). The T1-1 site is a Ga top site on a Ga atom that is displaced upward in the surface reconstruction of $(\sqrt{3} \times \sqrt{3})R30^\circ$ GaN (0001), and the T1-2 site is a Ga top site on a Ga atom that is not displaced upward after the surface reconstruction. The Gb-1 site is a Ga bridge site between two Ga atoms which are not displaced upward after surface reconstruction, and the Gb-2 site is adjacent to a Ga atom that is displaced upward after surface reconstruction. Lastly, the H3-1 and H3-2 sites are hollow sites, and the T4 site is a N top site.

As mentioned previously, the relative potential energies for a Ga adatom on $(\sqrt{3} \times \sqrt{3})R30^\circ$ GaN (0001) at T1, H3, and T4 are 0.75, 0.25, and 0 eV, respectively. The relative potential energies for a Ga adatom on the $(2\sqrt{3} \times 2\sqrt{3})R30^\circ$ GaN (0001) surface are shown in Fig. 8(b). The T1 sites remain the least stable, and T4 remains the most stable site. However, we now find that the T1-1 and T1-2 sites are energetically inequivalent, and the T1-1 site is significantly less stable than the T1-2 site. We also find that the Ga bridge sites are energetically inequivalent which affects the diffusion barriers. The diffusion path from H3-1 to T4 has no diffusion barrier and a potential energy difference of 0.23 eV, which corresponds to what we observed when studying Ga adatom diffusion on the $(\sqrt{3} \times \sqrt{3})R30^\circ$ surface. However, using a larger surface cell, we can see that there is a metastable site at H3-2, and an additional path for diffusion can occur along T4 and H3-2 sites. The diffusion path from H3-2 to T4 has a diffusion barrier of 0.38 eV, corresponding to a diffusion

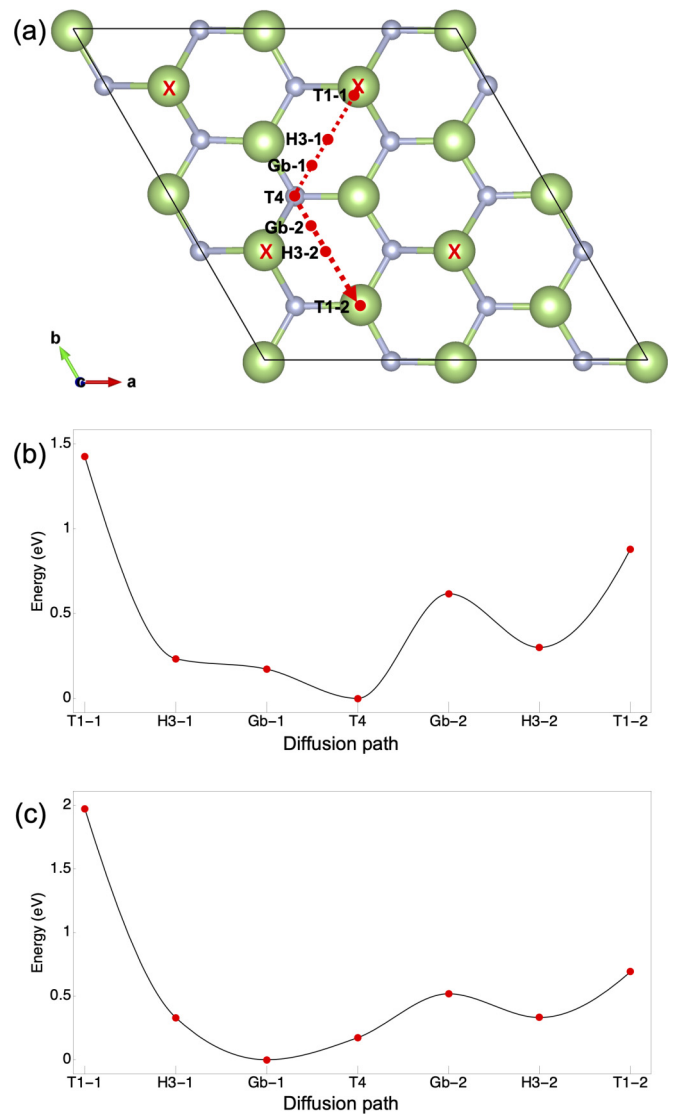


FIG. 8. The diffusion path of the Ga and La adatom on the $(2\sqrt{3} \times 2\sqrt{3})R30^\circ$ GaN (0001) surface is shown in (a) where the red crosses mark the surface Ga atoms that are displaced upwards in the surface reconstruction. The energy profile for the Ga adatom along the diffusion path is shown in (b) and the same for the La adatom is shown in (c).

rate of approximately 10^{-6} and 10^{-11} s at room temperature and 750°C , respectively. Diffusion in the reverse direction has a barrier of 0.62 eV, corresponding to a diffusion rate of approximately 10^{-2} and 10^{-9} s at room temperature and 750°C , respectively.

We found that the relative potential energies of a La adatom at T1, H3, and T4 on $(\sqrt{3} \times \sqrt{3})R30^\circ$ GaN (0001) are 0.95, 0.34, and 0 eV. The relative potential energies for a La adatom on the $(2\sqrt{3} \times 2\sqrt{3})R30^\circ$ GaN (0001) surface are shown in Fig. 8(c). Like our findings using the $(\sqrt{3} \times \sqrt{3})R30^\circ$ GaN (0001) surface, the T1-1 site is the least stable site. However, on the larger surface, we find the Gb-1 site is the most stable, whereas La is most stable on the T4 site on the $(\sqrt{3} \times \sqrt{3})R30^\circ$ GaN (0001) surface. Like what we found with the Ga adatom, the T1-1 and T1-2 sites and Gb-1 and Gb-2

sites are energetically inequivalent. Diffusion from Gb-1 to H3-2 has a barrier of 0.52 eV, corresponding to a diffusion rate of approximately 10^{-4} and 10^{-10} s at room temperature and 750 °C, respectively. Diffusion in the reverse direction has a barrier of 0.19 eV, corresponding to a diffusion rate of approximately 10^{-9} and 10^{-11} s at room temperature and 750 °C, respectively. Like the Ga adatom, there is a metastable site at H3-2, and diffusion can occur along Gb-1 and H3-2 sites.

F. Single Ga and La adatom surface exchange on $(2\sqrt{3}\times 2\sqrt{3})R30^\circ$ GaN surface

We also test if the energy barrier for exchanging a Ga or La adatom with a Ga atom from the surface layer of GaN would change if we increase the surface area of the GaN slab. When using a $(2\sqrt{3}\times 2\sqrt{3})R30^\circ$ GaN slab, the exchange energy barrier for a Ga adatom increases to 2.14 eV, and for a La adatom, it increases to 1.71 eV. We also find that, when the La adatom exchanges with any of the adjacent surface Ga atoms, the energy decreases by 0.89 eV on the $(2\sqrt{3}\times 2\sqrt{3})R30^\circ$ slab compared with 1.73 eV on the $(\sqrt{3}\times \sqrt{3})R30^\circ$ periodic cell. To determine what causes the energy barriers to increase, we compare the energies of the Ga and La adatoms on the $(\sqrt{3}\times \sqrt{3})R30^\circ$ and $(2\sqrt{3}\times 2\sqrt{3})R30^\circ$ GaN surfaces by subtracting the energy of the bare GaN slab from the slab with an adatom. We found that the Ga and La adatoms on the $(2\sqrt{3}\times 2\sqrt{3})R30^\circ$ GaN slab are lower in energy by 0.51 and 1.00 eV, respectively. This indicates that both adatoms are more stable on the $(2\sqrt{3}\times 2\sqrt{3})R30^\circ$ surface, which increases the exchange energy barriers.

G. Ga adsorption

Until now, we have considered the surface reconstruction corresponding to GaN grown under N-rich conditions. However, the surface of GaN grown under N-rich conditions is typically rough, whereas GaN grown in Ga-rich conditions is smooth and yields a higher-quality film [19]. Hence, we consider what happens if we increase the Ga coverage to gain insight into the structure of the Ga-rich GaN surface. We use the $(\sqrt{3}\times \sqrt{3})R30^\circ$ supercell and incrementally increase the number of Ga adatoms on a bulk-terminated GaN (0001) surface one atom at a time, up to eight Ga atoms. Each monolayer is made up of three Ga atoms, and for example, we denote six Ga adatoms as 2 ML and eight Ga adatoms as 2.7 ML. We calculate the reaction energy using the following equation:

$$E_{\text{adsorption}} = E_{\text{GaN}}^{\text{slab}} - E_{\text{GaN}}^{\text{bare}} - N_{\text{Ga}}(E_{\text{Ga}} + \mu_{\text{Ga}}),$$

where $E_{\text{adsorption}}$ is the adsorption energy of a Ga adatom, $E_{\text{GaN}}^{\text{slab}}$ is the energy of the GaN slab with the Ga adatoms, $E_{\text{GaN}}^{\text{bare}}$ is the energy of the bare GaN slab, N_{Ga} is the number of Ga adatoms, E_{Ga} is the energy of a bulk Ga atom, and μ_{Ga} is the chemical potential of orthorhombic bulk Ga (space group *Abma*). We calculate the formation energy of GaN to be 0.97 eV, which is lower than the experimental value of 1.15 eV [45]. The plot of the adsorption energy as a function of the Ga chemical potential is shown in Fig. 9(a). In the N-rich regime, when μ_{Ga} is -1.0 to -0.6 eV, we find that the bare GaN surface is the most stable surface arrangement and that the adsorption en-

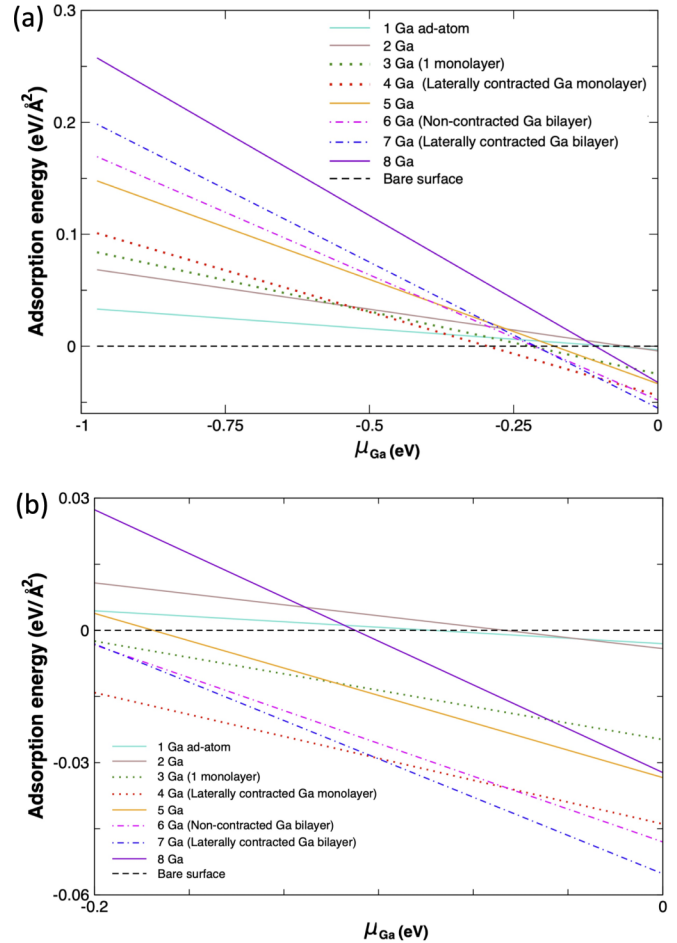


FIG. 9. Adsorption energy of Ga adatoms on the $(\sqrt{3}\times \sqrt{3})R30^\circ$ GaN (0001) surface with respect to the Ga chemical potential for (a) the full chemical potential and (b) the Ga-rich region. The environment is Ga-rich near 0 eV and N-rich near 0.97 eV.

ergy increases with each additional Ga adatom. Hence, in the N-rich regime, the bare GaN surface is the most stable surface arrangement. A closer look at the Ga-rich regime is shown in Fig. 9(b). In the Ga-rich regime, starting with the bare GaN (0001) surface, we find that the adsorption energy decreases with each additional Ga adatom until the fifth Ga adatom is introduced, which increases the adsorption energy. We then observe a similar pattern in which the adsorption energy decreases with the addition of the sixth and seventh Ga adatoms and then increases with the addition of the eighth Ga adatom. This suggests that simply adding Ga atoms does not lower the energy of the surface. Instead, the energy is lowered until a low-energy arrangement is formed, and once an additional Ga is added, the surface energy increases. We found that the adsorption energy is degenerate when $\frac{4}{3}$, 2, and $\frac{7}{3}$ ML of Ga is on the GaN surface because the difference in energy between configurations is within kT . However, experimental evidence suggests that, when GaN is grown under Ga-rich conditions, 2–3 ML of fluidlike Ga is present at the surface. There is also experimental evidence showing a “1 × 1” reconstruction on the GaN surface [20], which is only present in the $\frac{4}{3}$ and $\frac{7}{3}$ ML arrangements. Additionally, it has been previously reported that a 2.3 ML coverage is the lowest energy arrangement,

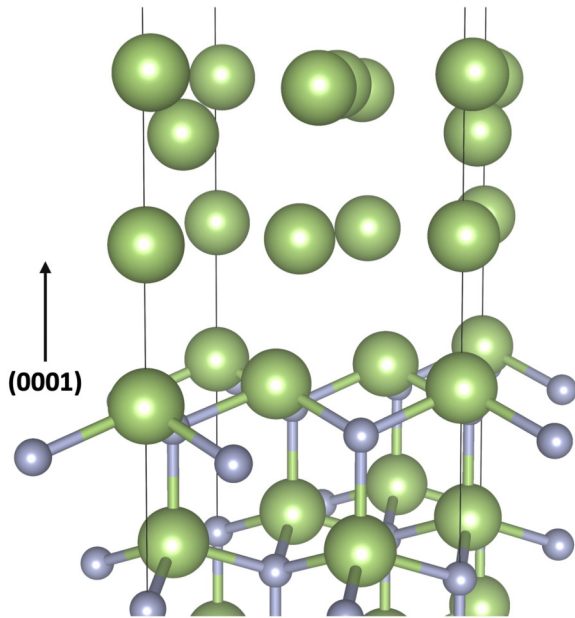


FIG. 10. Surface reconstruction of the laterally contracted Ga bilayer on $(\sqrt{3}\times\sqrt{3})R30^\circ$ GaN (0001). The large green spheres and small gray spheres are Ga and N atoms, respectively.

so we take a closer look at this arrangement [20,21]. The arrangement of 2.3 ML of Ga adatoms is also known as the laterally contracted Ga bilayer [21]. In the laterally contracted Ga bilayer, the Ga adlayer directly above the GaN surface is composed of three Ga atoms which are directly above the Ga atoms composing the GaN surface. The topmost layer of the Ga bilayer is composed of four Ga atoms. In the structure we determined, one of these Ga atoms is lower than the others by approximately 1 Å [Fig. 10]. Our structure differs from those found in previous studies [21,22], where one of the topmost Ga atoms is raised above the others by 0.17 Å. In our case, instead of one Ga atom being displaced upward toward the vacuum region, one Ga atom sinks into the bilayer.

The Ga bilayer arrangement determined by Northrup *et al.* [21] used the LDA exchange correlation functional, and we have used the PBE-GGA exchange correlation functional in this paper. To better compare our results, we considered the reconstruction of the $(\sqrt{3}\times\sqrt{3})R30^\circ$ GaN (0001) with a laterally contracted Ga bilayer using LDA. The Ga bilayer arrangement determined using LDA is like the arrangement found using GGA, with the main difference being that one Ga atom is lower than the others by 0.85 Å. Typically, the GGA functional tends to overestimate the size of atoms, while the LDA functional underestimates them, which may explain why the displacement is smaller for the LDA result. We conclude that the choice of functional did not result in a different general arrangement of the laterally contracted Ga bilayer. To roughly compare the energy difference between the two configurations, we simulated the surface arrangement that was previously reported. We found that our arrangement was lower in energy by 4 meV/Å² when we used either the GGA or LDA functional and conclude the two arrangements are energetically degenerate, despite the difference in atomic arrangement, as would be expected for a fluidlike phase.

H. La diffusion through Ga bilayer

The charge transfer between the La adatom and the surface Ga atoms suggests the possibility of forming LaGa₂ on the GaN surface. This also shows that the surface Ga atoms can participate in bonding with adatoms. In the $(\sqrt{3}\times\sqrt{3})R30^\circ$ structure with the Ga bilayer, there are 10 Ga atoms that can participate in bonding at the (0001) surface. This is the ideal number of Ga for forming LaGa₂ on GaN. The radius of a La atom, shown in Table I, is like that of Ga. Hence, La could be small enough to diffuse through the Ga bilayer. We studied the diffusion of a La adatom in the Ga bilayer to determine if an exchange with a surface Ga atom remains energetically favorable with the presence of the Ga bilayer. In the first case [Fig. 11(a)], all Ga atoms from the Ga bilayer are included in the calculations, and in the second case [Fig. 11(b)], we assume that one Ga atom from the Ga bilayer has evaporated and remove it. We exchanged the La adatom with a Ga atom in the topmost layer of the Ga bilayer (L1), the second layer of the Ga bilayer (L2), a Ga atom from the top GaN layer (L3), and then a Ga atom from the second GaN layer (L4). We then used the cNEB method to calculate the energy barriers for the transition between each layer. The barrier from L3 to L4 could not be determined in both cases because the geometries required for this transition were unstable. We believe this issue arose because the bulk region limits the space available for the La and Ga atoms to move and creates an unstable structure during the transition. Since a La atom in L4 is also the highest energy structure in both cases, we assume this transition is unlikely.

The La exchange from L0 into L1 lowers the energy by 0.20 eV with a transition energy barrier of 0.15 eV, and a subsequent exchange into L2 increases the energy by 0.55 eV with a transition energy barrier of 1.95 eV. Hence, an exchange with a top Ga atom in the Ga bilayer is energetically favorable, but a second exchange is not. An exchange into L3 is lower by 0.87 eV with a transition energy barrier of 0.27 eV, indicating that an exchange with a surface Ga is still favorable even with a Ga bilayer. An exchange into L4 is higher in energy by 1.90 eV, suggesting that diffusion of La into GaN is unlikely. In the second case, an exchange from L1 into L2 increases the energy by 0.09 eV with a transition energy barrier of 1.20 eV. An exchange into L3 lowers the energy by 0.73 eV, also indicating a La exchange with a surface Ga atom remains favorable. Lastly, an exchange into L4 increases the energy by 1.68 eV, suggesting this transition is unlikely.

Our results are like those previously reported for the Y [35] and B [31] atoms. However, for Al, it appears that diffusion further into the GaN bulk remains energetically favorable [34], whereas in our case, the diffusion past the top layer of GaN is not. We attribute this to La being a larger atom than Al.

The energy barriers for each transition determined using the cNEB method are shown in Figs. 11(a) and 11(b). In both cases, the lowest energy configuration occurs when the La atom is in L3. However, the transition from L1 to L2 contains the highest energy barrier. This energy barrier is 1.95 eV in the first case and 1.20 eV in the second case. These transition barriers are comparable with those determined experimentally for Si and Mn in GaN, which are 1.5 eV [46] and 1.8 eV [47], respectively. As La atoms are introduced, they can diffuse

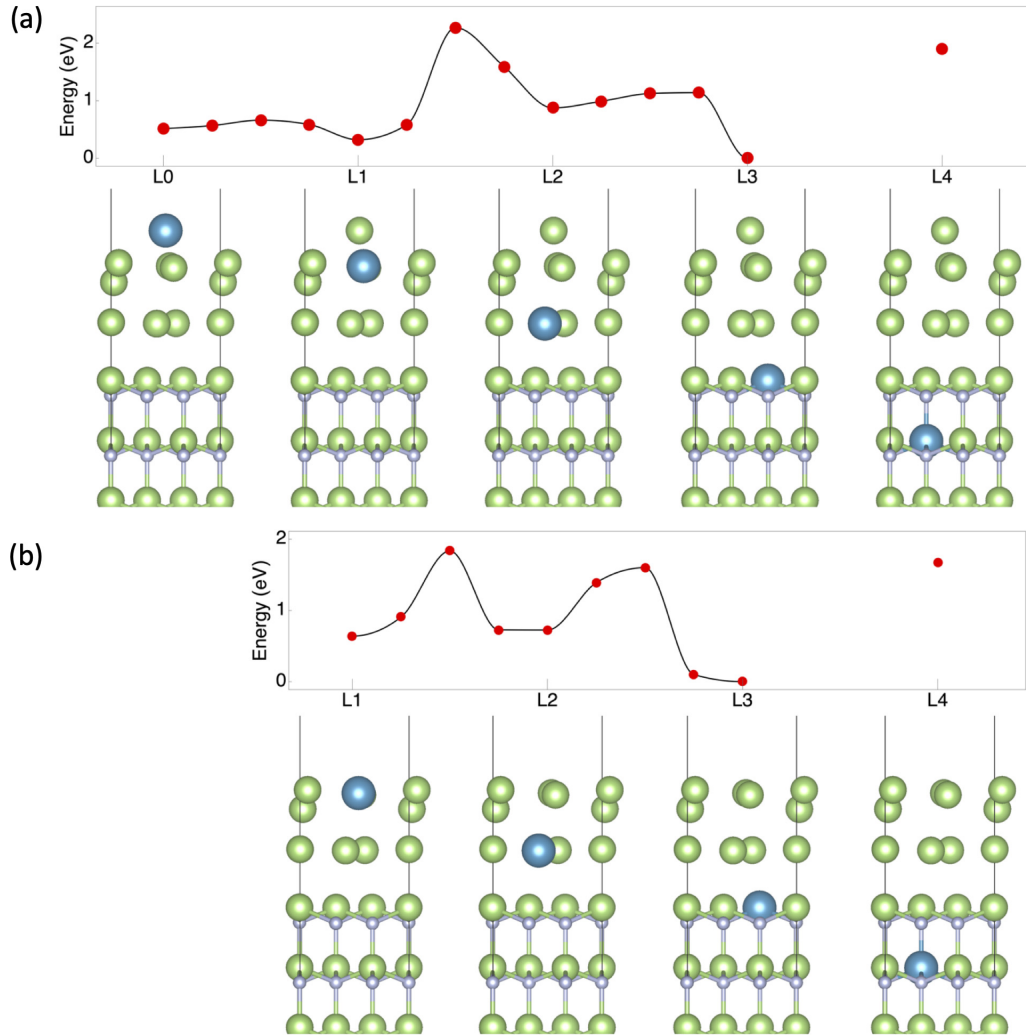


FIG. 11. Transitions calculated using the cNEB method and the atomic arrangement at each step during the diffusion of a La adatom through the Ga bilayer. In the first case (a) the number of Ga atoms does not change with the addition of La and in the second case (b) it is assumed that one Ga atom has evaporated once La adatom is introduced. The lowest energy adsorption site, L3 in both cases, is defined as 0 eV. The large green spheres, small gray spheres, and large blue sphere are Ga, N, and La atoms, respectively.

through the Ga bilayer and replace the Ga atoms in the top GaN layer to form a layer of LaN, and then the La atoms can accumulate in the Ga bilayer to form LaGa₂.

IV. CONCLUSIONS

Using DFT, we have studied the geometric and electronic properties of the reconstructed GaN (0001) surface and compared the effects of using LDA or GGA for different size simulation cells. We have investigated the diffusion of Ga and La atoms on the $(\sqrt{3}\times\sqrt{3})R30^\circ$ and $(2\sqrt{3}\times2\sqrt{3})R30^\circ$ GaN surfaces and compare our results with previously reported values for the diffusion of rare-earth atoms on GaN. On both GaN surfaces, we find a low migration barrier for a Ga adatom along T4 sites, resulting in a fast diffusion rate. For a La adatom on the $(\sqrt{3}\times\sqrt{3})R30^\circ$ GaN surface, we find a low migration barrier along the H3 and T4 sites, and on the $(2\sqrt{3}\times2\sqrt{3})R30^\circ$ GaN surface, we find a low barrier along the Gb-1 and H3-2 sites. Additionally, we have found a low potential energy barrier for the surface exchange reaction

between a La adatom and a surface Ga atom and determined that an exchange reaction is energetically favorable on the $(\sqrt{3}\times\sqrt{3})R30^\circ$ and $(2\sqrt{3}\times2\sqrt{3})R30^\circ$ GaN surfaces. Our findings support the possibility that rare-earth atoms likely spontaneously form rare-earth nitrides at the GaN surface. We found that charge is transferred from the La adatom to the surface Ga atoms, indicating a Zintl-like charge transfer. When the La atom exchanges positions with a surface Ga atom, we still observe Zintl-like charge transfer, and the average distance between the La and Ga atoms is 3.2 Å, which resembles the 3.35 Å spacing present in LaGa₂. We have also determined that a contracted Ga bilayer containing 2.3 ML of Ga on GaN is the lowest energy structure under Ga-rich conditions, which supports previous reports. However, we have found a different arrangement of the bilayer in which a single Ga atom has a downward displacement of 0.85 Å, where previous reports show a downward displacement of three Ga atoms by 0.17 Å. While the structures are energetically equivalent, the difference in the arrangement of the Ga bilayer may still affect results of modeling diffusion through

the Ga bilayer. Lastly, we modeled the diffusion of La through the Ga bilayer and find that it is favorable for the La adatom to migrate to the surface of GaN and form a rare-earth nitride. It is apparent that surface Ga atoms can participate in bonding with adatoms, and the addition of a Ga bilayer presents an ideal number of Ga atoms to form LaGa₂ on the surface through the diffusion of La.

ACKNOWLEDGMENTS

We thank Donghan Shin, Agham Posadas, and Tobias Hadamek for many insightful discussions and critical reading of the paper. This paper was supported by the National Science Foundation under Award No. DMR-1507970 and by the Air Force Office of Scientific Research under Grant No. FA9550-18-1-0053.

-
- [1] F. Roccaforte, P. Fiorenza, G. Greco, R. Lo Nigro, F. Giannazzo, F. Iucolano, and M. Saggio, *Microelectron. Eng.* **187–188**, 66 (2018).
- [2] L. Liu and J. H. Edgar, *Mater. Sci. Eng. R: Rep.* **37**, 61 (2002).
- [3] S. J. Pearton, B. S. Kang, S. Kim, F. Ren, B. P. Gila, C. R. Abernathy, J. Lin, and S. N. G. Chu, *J. Phys.: Condens. Matter* **16**, R961 (2004).
- [4] J. Kwo and M. Hong, in *Advanced Gate Stacks for High-Mobility Semiconductors. Advanced Microelectronics*, edited by A. Dimoulas, E. Gusev, P. C. McIntyre, and M. Heyns (Springer, Berlin, Heidelberg, 2007), Vol 27, pp. 229–256.
- [5] W. H. Chang, P. Chang, T. Y. Lai, Y. J. Lee, J. Kwo, C. H. Hsu, and M. Hong, *Cryst. Growth Des.* **10**, 5117 (2010).
- [6] G. Y. Adachi and N. Imanaka, *Chem. Rev.* **98**, 1479 (1998).
- [7] V. V. Afanas'ev, M. Badylevich, A. Stesmans, A. Laha, H. J. Osten, A. Fissel, W. Tian, L. F. Edge, and D. G. Schlom, *Appl. Phys. Lett.* **93**, 192105 (2008).
- [8] M. Badylevich, S. Shamulia, V. V. Afanas'ev, A. Stesmans, A. Laha, H. J. Osten, and A. Fissel, *Appl. Phys. Lett.* **90**, 252101 (2007).
- [9] P. Y. Chen, A. B. Posadas, S. Kwon, Q. Wang, M. J. Kim, A. A. Demkov, and J. G. Ekerdt, *J. Appl. Phys.* **122**, 215302 (2017).
- [10] T. Hadamek, D. Shin, A. B. Posadas, A. A. Demkov, S. Kwon, Q. Wang, and M. Kim, *Appl. Phys. Lett.* **111**, 142901 (2017).
- [11] P. Y. Chen, T. Hadamek, S. Kwon, F. Al-Quaiti, A. B. Posadas, M. J. Kim, A. A. Demkov, and J. G. Ekerdt, *J. Vac. Sci. Technol. A* **38**, 012403 (2020).
- [12] J. W. Johnson, B. Luo, F. Ren, B. P. Gila, W. Krishnamoorthy, C. R. Abernathy, S. J. Pearton, J. I. Chyi, T. E. Nee, C. M. Lee, and C. C. Chuo, *Appl. Phys. Lett.* **77**, 3230 (2000).
- [13] R. Mehandru, B. Luo, J. Kim, F. Ren, B. P. Gila, A. H. Onstine, C. R. Abernathy, S. J. Pearton, D. Gotthold, R. Birkhahn, B. Peres, R. Fitch, J. Gillespie, T. Jenkins, J. Sewell, D. Via, and A. Crespo, *Appl. Phys. Lett.* **82**, 2530 (2003).
- [14] M. Esposito, S. Krishnamoorthy, D. N. Nath, S. Bajaj, T. H. Hung, and S. Rajan, *Appl. Phys. Lett.* **99**, 133503 (2011).
- [15] J. Son, V. Chobpattana, B. M. McSkimming, and S. Stemmer, *Appl. Phys. Lett.* **101**, 102905 (2012).
- [16] M. A. Moram, M. J. Kappers, Z. H. Barber, and C. J. Humphreys, *J. Cryst. Growth* **298**, 268 (2007).
- [17] J. D. Greenlee, A. Nath, T. J. Anderson, B. N. Feigelson, A. D. Koehler, K. D. Hobart, R. D. Dupuis, T. Detchprohm, S. C. Shen, and F. J. Kub, *ECS J. Solid State Sci. Technol.* **6**, Q3067 (2017).
- [18] A. A. Demkov, H. Seo, X. Zhang, and J. Ramdani, *Appl. Phys. Lett.* **100**, 071602 (2012).
- [19] V. M. Bermudez, *Surf. Sci. Rep.* **72**, 147 (2017).
- [20] A. R. Smith, R. M. Feenstra, D. W. Greve, M. S. Shin, M. Skowronski, J. Neugebauer, and J. E. Northrup, *J. Vac. Sci. Technol. B* **16**, 2242 (1998).
- [21] J. E. Northrup, J. Neugebauer, R. M. Feenstra, and A. R. Smith, *Phys. Rev. B* **61**, 9932 (2000).
- [22] A. L. Rosa and J. Neugebauer, *Phys. Rev. B* **73**, 205314 (2006).
- [23] C. E. Dreyer, A. Janotti, and C. G. Van de Walle, *Phys. Rev. B* **89**, 081305(R) (2014).
- [24] K. Rapcewicz, M. B. Nardelli, and J. Bernholc, *Phys. Rev. B* **56**, R12725(R) (1997).
- [25] G. Kresse and J. Furthmüller, *Phys. Rev. B* **54**, 11169 (1996).
- [26] P. E. Blöchl, *Phys. Rev. B* **50**, 17953 (1994).
- [27] H. Neumann, *Cryst. Res. Technol.* **30**, 910 (1995).
- [28] H. Schulz and K. H. Thiemann, *Solid State Commun.* **23**, 815 (1977).
- [29] D. Shin, T. Hadamek, and A. A. Demkov, *Phys. Rev. Mater.* **3**, 044607 (2019).
- [30] K. Karch, J.-M. Wagner, and F. Bechstedt, *Phys. Rev. B* **57**, 7043 (1998).
- [31] L. Palomino-Rojas, R. García-Díaz, G. H. Coccoletzi, and N. Takeuchi, *J. Cryst. Growth* **338**, 62 (2012).
- [32] J. Guerrero-Sánchez, F. Sánchez-Ochoa, G. H. Coccoletzi, J. F. Rivas-Silva, and N. Takeuchi, *Thin Solid Films* **548**, 317 (2013).
- [33] J. A. Rinehimer, M. Widom, J. E. Northrup, and R. M. Feenstra, *Phys. Status Solidi Basic Res.* **245**, 920 (2008).
- [34] Z. Qin, Z. Xiong, G. Qin, and Q. Wan, *J. Appl. Phys.* **114**, 194307 (2013).
- [35] J. Guerrero-Sánchez, G. H. Coccoletzi, J. F. Rivas-Silva, and N. Takeuchi, *Comput. Mater. Sci.* **106**, 155 (2015).
- [36] J. Guerrero-Sánchez, G. H. Coccoletzi, J. F. Rivas-Silva, and N. Takeuchi, *Appl. Surf. Sci.* **268**, 16 (2013).
- [37] R. González-Hernández, W. López-Pérez, M. G. Moreno-Armenta, and J. A. Rodríguez M., *Phys. Rev. B* **81**, 195407 (2010).
- [38] V. Heine, *J. Phys. C Solid State Phys.* **1**, 222 (1968).
- [39] C. Zheng, H. Mattausch, and A. Simon, *Z. Kristallogr.* **216**, 531 (2001).
- [40] F. Cheviré and F. J. DiSalvo, *J. Alloys Compd.* **457**, 372 (2008).
- [41] J. E. Mahan, *Physical Vapor Deposition of Thin Films* (Wiley, New York, 2000).
- [42] T. Zywiets, J. Neugebauer, and M. Scheffler, *Appl. Phys. Lett.* **73**, 487 (1998).

- [43] J. Neugebauer, T. K. Zywietz, M. Scheffler, J. E. Northrup, H. Chen, and R. M. Feenstra, *Phys. Rev. Lett.* **90**, 056101 (2003).
- [44] G. Henkelman, B. P. Uberuaga, and H. Jónsson, *J. Chem. Phys.* **113**, 9901 (2000).
- [45] J. Elsner, M. Haugk, G. Jungnickel, and T. Frauenheim, *Solid State Commun.* **106**, 739 (1998).
- [46] R. Jakiela, A. Barcz, E. Dumiszewska, and A. Jagoda, *Phys. Status Solidi C* **3**, 1416 (2006).
- [47] R. Jakiela, K. Gas, M. Sawicki, and A. Barcz, *J. Alloys Compd.* **771**, 215 (2019).
- [48] P. Villars and K. Cenzual, *Pearson's Crystal Data: Crystal Structure Database for Inorganic Compounds (on DVD)* (ASM International, Materials Park, OH, 2017).